Research Article: New Research | Cognition and Behavior

Color tuning of face-selective neurons in macaque inferior temporal cortex

This Early Release article has been peer-reviewed and accepted, but has not been through the composition and copyediting processes. The final version may differ slightly in style or formatting and will contain links to any extended data.

Alerts: Sign up at www.eneuro.org/alerts to receive customized email alerts when the fully formatted version of this article is published.

1   Color tuning of face-selective neurons in macaque inferior temporal cortex

2

3   Short title: Color tuning of face-cells in macaque IT cortex

4

5   Marianne Duyck, Laboratory of Sensorimotor Research, National Eye Institute, National Institutes of
6   Health, Bethesda, MD 20982-4435
7   Audrey L.Y. Chang, Laboratory of Sensorimotor Research, National Eye Institute, National Institutes of
8   Health, Bethesda, MD 20982-4435
9   Tessa J. Gruen, Laboratory of Sensorimotor Research, National Eye Institute, National Institutes of
10   Health, Bethesda, MD 20982-4435
11   Lawrence Y. Tello, Laboratory of Sensorimotor Research, National Eye Institute, National Institutes of
12   Health, Bethesda, MD 20982-4435
13   Serena Eastman, Laboratory of Sensorimotor Research, National Eye Institute, National Institutes of
14   Health, Bethesda, MD 20982-4435
15   Joshua Fuller-Deets, Laboratory of Sensorimotor Research, National Eye Institute, National Institutes of
16   Health, Bethesda, MD 20982-4435
17   Bevil Conway, Laboratory of Sensorimotor Research, National Eye Institute, National Institutes of Health,
18   Bethesda, MD 20982-4435

19

20   B.C designed the research, T.J.G, L.Y.T and S.E performed the research, M.D analyzed the data, A.L.Y.C
21   and M.D did the population information analysis, J.FD generated the stimuli and the handled the
22   experimental display code, B.C and M.D wrote the paper.

23

24   bevil@nih.gov

25

26   12 Figures
27   2 Tables
28   0 Multimedia
29   234 Words in the abstract
30   120 Words in the significance statement
31   625 Words in introduction
32   1501 Words in discussion

33

42

43

What role does color play in the neural representation of complex shapes? We approached the question by measuring color responses of face-selective neurons, using fMRI-guided microelectrode recording of the middle and anterior face patches of inferior temporal cortex (IT) in rhesus macaques. Face-selective cells responded weakly to pure color (equiluminant) photographs of faces. But many of the cells nonetheless showed a bias for warm colors when assessed using images that preserved the luminance contrast relationships of the original photographs. This bias was also found for non-face-selective neurons. Fourier analysis uncovered two components: the first harmonic, accounting for most of the tuning, was biased towards reddish colors, corresponding to the L>M pole of the L-M cardinal axis. The second harmonic showed a bias for modulation between blue and yellow colors axis, corresponding to the S-cone axis. To test what role face-selective cells play in behavior, we related the information content of the neural population with the distribution of face colors. The analyses show that face-selective cells are not optimally tuned to discriminate face colors, but are consistent with the idea that face-selective cells contribute selectively to processing the green-red contrast of faces. The research supports the hypothesis that color-specific information related to the discrimination of objects, including faces, is handled by neural circuits that are independent of shape-selective cortex, as captured by the multi-stage parallel processing framework of IT (Lafer-Sousa and Conway, Nature Neuroscience, 2013).

Significance: *Does the brain encode face-specific color signals, such as those related to health and emotion, through color responses of face-selective neurons? This paper addresses this question by providing the first, to our knowledge, quantitative measurements of the color-tuning of face-selective cells. Face-selective cells are not very responsive to pure color (equiluminant) pictures of faces. But both face-selective and non-face-selective cells are biased for warm colors. Information analysis shows that face-selective cells are not optimally tuned to discriminate face colors but suggests that the cells may contribute to discriminating the reddish component of faces. Alternatively, face-cell color tuning may reflect a broader adaptation of IT for the detection of objects, which are, in general, characterized by warmer coloring compared to backgrounds.*

What role does color play in the neural representation of objects? Some cells in inferior temporal cortex (IT) are shape selective, and many of these cells are also modulated by color (Komatsu and Ideura, 1993; Edwards et al., 2003). Do shape-selective IT cells play a role in discriminating among the typical colors of the shapes to which they are tuned? We take up this question by measuring the color responses of face-selective neurons in fMRI-identified face patches of macaque monkey; we evaluate the possible role of the color tuning by relating the information content at the neural population level with the distribution of face colors (Xiao et al., 2017).

The extent to which face-selective neurons in IT are color-tuned is unsettled. A widespread but not universal assumption is that face cells do not carry color information. The assumption is supported by the observation that luminance contrast is by itself sufficient for face recognition (Kemp et al., 1996; Sinha et al., 2006) and the lack of cross face/color adaptation in psychophysical experiments (Yamashita et al., 2005). Consequently, many studies of face perception use exclusively colorless images (Kanwisher et al., 1997; Ohayon et al., 2012). But while color is not essential for determining face identity, color nonetheless relays important information related to social communication, about health, emotion, and sex (Setchell and Wickings, 2005; Changizi et al., 2006; Waitt et al., 2006; Nestor and Tarr, 2008; Gerald et al., 2009; Leopold and Rhodes, 2010; Webster and MacLeod, 2011; Lefevre et al., 2013; Nakajima et al., 2017; Petersdorf et al., 2017). Moreover, faces viewed under low pressure sodium light (which

2

87   impairs retinal mechanisms for encoding color) have a paradoxical appearance: they appear green,
88   regardless of race (Hasantash et al., 2019). Such seemingly anti-Bayesian phenomena may arise if neural
89   representations and how they are decoded are optimal with respect to the statistics of the environment
90   (Wei and Stocker, 2015); efficient coding thus predicts a neural population whose tuning curves best
91   discriminate among the most common face colors (Hasantash et al., 2019). One possibility is that this
92   face-relevant color information is encoded by face-selective neurons.

93   To what extent could face-selective cells discriminate among face colors? Two studies have glanced the
94   question. One found no sensitivity to color among face-selective neurons (Perrett et al., 1982). The
95   other study found that of 22 cells, some showed higher firing rates for naturally colored face
96   photographs compared to un-naturally colored photographs (Edwards et al., 2003), suggesting that face-
97   selective neurons carry color signals. Quantitative measurements of color-tuning functions of face-
98   selective neurons have, to our knowledge, not been made, which precludes an answer to the question.

99   The discrimination potential of a population can be estimated by the Fisher information, which depends
100   on the distribution of tuning peaks, tuning widths, and amplitude modulation across the neural
101   population (Ganguli and Simoncelli, 2010) (**Figure 1**). If a population activity is to be used to discriminate
102   a given attribute, efficient coding predicts that its Fisher information should reflect the distribution of
103   the attribute in the environment (Wei and Stocker, 2015). If face-selective cells were being used to
104   discriminate face color, then the Fisher information across the population should reflect the natural
105   distribution of face colors. Here we use fMRI-guided electrode recording of neurons in the middle and
106   anterior face patches of macaque monkeys. We discovered that face-selective cells, as a population,
107   were biased for warm colors. The resulting Fisher Information shows a striking dip that coincides with
108   the peak in the distribution of face colors documented in a large database of measurements of human
109   face colors (Xiao et al., 2017). The results suggest that face-selective neurons are not optimally
110   distributed to enable the discrimination of face colors. We discuss what role color responses of face-
111   selective cells may play in visual processing.

112   **Methods**

113   *Subjects*
114   Three male rhesus macaques (*Macaca mulatta*), weighing 8-10 kgs, were implanted with an MRI-
115   compatible plastic (Delrin) chamber and headpost. Surgical implantation protocol has been described
116   previously (Lafer-Sousa and Conway, 2013). Designation of the subjects are M1 (monkey 1), M2
117   (monkey 2), and M3 (monkey 3). Monkeys 1 and 3 (M1, M3) had chambers over the right hemisphere;
118   Monkey 2 (M2) had a chamber on the left hemisphere. All procedures were approved by the Animal
119   Care and Use Committee of the National Eye Institute and complied with the regulations of the National
120   Institutes of Health.

121   *Functional Imaging targeting of Face Patches*
122   The fMRI procedures we use for localizing face patches have been described (Tsao et al., 2006; Lafer-
123   Sousa and Conway, 2013; Rosenthal et al., 2018). Two of the animals (M1, M2) are the same as the
124   animals used in Lafer-Sousa and Conway (2013); the face-patch data and color-tuning data are the same
125   as in the earlier reports. Here, we present an analysis of the fMRI color-tuning data restricted to the face
126   patches of inferior temporal cortex. All monkeys were scanned at the Massachusetts General Hospital
127   Martinos Imaging Center in a Siemens 3T Tim Trio scanner. Magnetic resonance images were acquired
128   with a custom-built four-channel magnetic resonance coil system with AC88 gradient insert, which

129   increases the signal-to-noise ratio by allowing very short echo times, providing 1-mm3 spatial resolution
130   and good coverage of the temporal lobe. We used standard echo planar imaging (repetition time = 2 s,
131   96 × 96 × 50 matrix, 1 mm^3 voxels; echo time = 13 ms). Monkeys were seated in a sphinx position in a
132   custom-made chair placed inside the bore of the scanner, and they received a juice reward for
133   maintaining fixation on a spot presented at the center of the screen at the end of the bore. An infrared
134   eye tracker (ISCAN) was used to monitor eye movements, and animals were only rewarded by juice for
135   maintaining their gaze within ~1 degree of the central fixation target. Magnetic resonance signal
136   contrast was enhanced using a microparticular iron oxide agent – MION (Feraheme, 8–10 mg per kg of
137   body weight, diluted in saline, AMAG Pharmaceuticals), injected intravenously into the femoral vein just
138   before scanning.

139   Visual stimuli were displayed on a screen subtending 41 by 31 dva, at 49 cm in front of the animal using
140   a JVC-DLA projector (1024 by 768 pixels). The subset of presented stimuli used here to localize face
141   patches consisted in achromatic square photographs of faces and body parts presented centrally on a
142   neutral gray screen (~25 cd.m^{-2}) and occupying 6 degrees. They were shown in 16 32-s blocks (16
143   repetition times per block, repetition time = 2 s, 2 images per repetition) presented in one run
144   sequence. The images were matched in average luminance to the neutral gray, maintaining roughly
145   constant average luminance (~25 cd.m^{-2}) throughout the stimulus sequence. For faces stimuli we used:
146   16 unique images front-facing of unfamiliar faces (8 human, 8 monkey) repeated twice within a block.
147   The bodies/body parts block comprised 32 unique images of monkey and human bodies (no
148   heads/faces) and body parts. Face patches were localized by contrasting responses to faces versus
149   responses to body parts. 18 runs were used to localize face patches in M1 and M2, and 16 runs were
150   used to localize face patches in M3.

151   *Physiological recordings*
152   A plastic grid was fitted to the inside of the recording chamber to enable us to reproducibly target
153   regions within the brain, following details reported previously (Conway et al., 2007). We used sharp
154   epoxy-coated tungsten electrodes (FHC), propelled using a hydraulic manual advancer (Narishige).
155   Voltage traces were digitized and saved with a Plexon MAP system (Plexon Inc., Dallas, TX). Spike
156   waveforms were sorted offline with the Plexon Offline Sorter, and single units were defined on the basis
157   of waveform and inter-spike interval.
158
159   Recordings were performed in a light-controlled room, with the animals seated in sphinx position.
160   Animals were acclimatized to head restraint in order to minimize head movement during recordings.
161   Animals maintained fixation on a spot on a monitor 57 cm away; the monitor was a CRT Barco
162   subtending 40 by 30 dva, operating at 85 Hz and at a resolution of 1024 by 768 pixels. Eye position was
163   monitored throughout the experiments using and infrared eye-tracker (ISCAN). The monitor was color
164   calibrated using a PR-655 SpectraScan Spectroradiometer (Photo Research Inc.); we achieved 14-bit
165   resolution for each phosphor channel using Bits++ (Cambridge Research Systems).
166
167   *Stimuli*
168   Screening stimuli consisted in 10 grayscale exemplars of each of the 14 following categories: animals,
169   buildings, human faces (front view), monkey faces (front view), human faces (3/4 view), monkey faces
170   (3/4 view), fruits, furniture, monkey bodies (no face), human bodies (no face), places, technology

4

171   objects, indoor places, natural scenes, vehicles. All stimuli were presented on a static luminance white
172   noise background of 7.5 by 7.5 degrees of visual angle.
173
174   Stimuli for the color-tuning experiments were exemplars of faces of unfamiliar humans and monkeys,
175   front or ¾ view (16 exemplar of frontal view and 8 of ¾ view for each species), fruits known to the
176   monkey (16 exemplars) and bodies/body parts (without head) of unfamiliar humans and monkeys (8
177   exemplars for each subcategory), yielding a total of 96 stimuli. For both sets of experiments using
178   colored stimuli (main condition in which the colored stimuli preserved the luminance contrast of the
179   original achromatic images, and the equiluminant condition) we defined 16 target hues equally spaced
180   along the CIELUV color space (values provided in Table 2). For the main condition (Figure 3), each pixel
181   value of the original achromatic image was remapped to the most saturated target color of the same
182   luminance value within the monitor gamut. For the equiluminant condition (Figure 9), each pixel value
183   of the original image was remapped to a pixel on the equiluminant plane, of the same hue as the target
184   but different saturation based on the pixel luminance (see Figure 9). Determination of equiluminance
185   was Judd-Vos corrected for the under-estimation of the contribution of S cones to the standard
186   luminosity function (Vos, 1978).

187   Note that one way of making false-colored images that has been used in some studies involves the
188   digital equivalent of superimposing a color filter over a black and white picture. In these images, the
189   white of the original image is replaced with a relatively saturated color. Although easy to generate,
190   these false-colored images are luminance compressed compared to the original image: the black in the
191   colored version remains the same luminance as the original, but the white is now a lower luminance
192   than the white in the original. Moreover, it is possible that the estimation of luminance for a given color
193   is inaccurate (see Conway, 2009 for a discussion). Such inaccuracies would introduce variability in the
194   luminance contrast among the different colored images generated using the color-filter method. For
195   example, when an achromatic image is falsely colored by applying a color filter, such that the white in an
196   original image is replaced with a given equiluminant color, the resulting set of differently colored,
197   photometrically equiluminant, versions of the image may have different luminance-contrast ranges that
198   systematically vary by hue: the red, yellow, and green images may have a higher luminance range than
199   the blue and purple images, because the contribution of S cones to the luminosity function is
200   underestimated. Thus, despite being ostensibly equiluminant, the brightest blue in the blue image may
201   be lower luminance than the brightest red in the red image, yet the black will be the same luminance in
202   both images. Variation in the responses to differently colored images created in this way cannot be
203   interpreted as color tuning because they may reflect variable sensitivity to the range of luminance
204   contrasts in the set of differently colored images. The method used presently mitigates the possible
205   impact of chromatic aberration and variability in macular pigmentation, and gives rise to images that are
206   more naturalistic: the images not only retain the luminance contrast of the original images but also
207   appear differently colored, rather than achromatic but viewed through a colored filter (see Golz and
208   MacLeod, 2002).
209

210   *Procedure*
211   One experimental session started by targeting a microelectrode to a face patch, recording a single unit
212   (selected online based on waveform), mapping the receptive field by hand, and choosing the visual-field
213   location that gave the highest response to the screening stimuli. Then we recorded the neural activity
214   while presenting the battery of screening stimuli. If a cell appeared face selective, we then recorded
215   responses to the colored stimuli presented in random order. During both screening and main

216 experiment stimuli were presented for 200 ms followed by a 200 ms blank (grey background). The
217 animals were rewarded by juice for maintaining their gaze within ~1 degree of the central fixation dot
218 for a specific duration (that duration usually started at 3 seconds but was decreased during the
219 experiment to adapt to the animal motivational state). Once a cell was found recording took place until
220 the animal stopped working thus yielding a variable number of trials per session, ranging from 369 to
221 15355 (IQR = [2945, 6755]). Across all sessions the number of repetitions for a given stimulus by hue
222 combination ranged between 0 and 15.

223 *Data Analysis*
224 *Response window*
225 The response of each neuron was quantified within a response window defined using the average
226 response to all stimuli, in 10 ms bins. The baseline firing rate of each cell was defined as the average
227 response from 50 ms before stimulus onset to 10 ms after stimulus onset. The response window for
228 each cell was determined as one continuous time period initiated when, within two consecutive time
229 bins, the neural response increased above 2.5 standard deviations above the baseline firing rate and
230 terminated either when the response dropped below 2.5 standard deviations of the baseline firing rate
231 in two consecutive bins or after 200 ms following the start of the response window (the shorter of the
232 two options was used). Cells were only included in the analysis if the response window was initiated
233 between 50 ms and 250 ms after stimulus onset, and if the neural response was excitatory (i.e. cells
234 showing suppressive responses to stimulus onset were not included).

235 *Face selectivity*
236 The present analysis focused on the color tuning of face-selective neurons. Face selectivity was assessed
237 using the following index:

$$FSI = \frac{R_{face} - mean(R_{bodies}, R_{fruits})}{|R_{face}| + |mean(R_{bodies}, R_{fruits})|}$$

238 Where R is the average response to stimulus, computed as the difference between the firing rate during
239 the response window and the firing rate during background. FSI values range from -1 to +1, with values
240 above 0 indicating a higher response to faces compared to bodies and fruits. All analyses, with one
241 exception, were restricted to neurons that showed an FSI $\geq$ 1/3, corresponding to a response to faces at
242 least twice than the response to other non-face stimuli. The exception was the last analysis (see Figure
243 12), in which we examined the relationship between hue preference and face selectivity. For that last
244 analysis we included an additional 61 cells (ML: 49 and AL: 12) that were recorded by targeting the same
245 face patches but had an FSI below 1/3. The total number of recorded cells was thus 234 (74% of the
246 targeted cells had an FSI of at least 1/3).

247 *Color Tuning*
248 To ensure that the results are not tainted by any cells that were not face selective, we focus on the
249 responses to color of those 173 cells that showed a face-selectivity index (FSI) greater than or equal to
250 1/3. An analysis of the color responses of the entire population of recorded neurons, which included
251 some cells with low FSI, is shown in Figure 12. In the color-tuning analyses we pooled responses across
252 the different face stimuli for each hue. Across all cells, pooling over stimuli, the number of trials per hue
253 ranged from 10 to 634 (IQR = [119, 277]).
254

255 **Significance.** We determined for each cell if there were significant variations in net firing rate across the
256 16 hues by computing the coefficient of variation (the ratio of the standard deviation across hues to the
257 mean) of the data recorded for the neuron compared to the distribution of coefficients of variation
258 obtained by 1000 permutations of hue labels. We considered color modulation to be significant when
259 the p-value was below $\alpha = 0.05$.

260

261 **Description: Vector sum.** Color responses were also quantified by determining the vector sum of the
262 color response. This analysis is enabled because hues are circularly distributed: we can consider the
263 neuron's response to a hue as a vector whose direction is the hue angle, and the vector norm is the
264 strength of the response within the response window compared to baseline. We normalized the vector
265 norms among hues so that the total sum over hues was one. The strength of the hue preference is
266 estimated by the direction and norm of the vector sum. Equation (1) describes the normalized vector
267 computed for each hue; we then sum these vectors using equation (2).

268 $$\vec{v}_{hue} = \frac{(FR_{hue} - \min(FR_{hues}))/(\max(FR_{hues}) - \min(FR_{hues}))}{\sum_{hue=1}^{16}[(FR_{hue} - \min(FR_{hues}))/(\max(FR_{hues}) - \min(FR_{hues}))]} * \begin{bmatrix} \cos\theta_{hue} \\ \sin\theta_{hue} \end{bmatrix} \quad (1)$$

269 $$\vec{v} = \sum_{hue=1}^{16} \vec{v}_{hue} \quad (2)$$

270 The preferred hue direction of the cell is the angle of $\vec{v}$. The strength of the hue preference is the norm
271 of $\vec{v}$, and can take values ranging from 0 (no hue preference) to 1. The norm of the vector sum therefore
272 reflects the narrowness of the color tuning.

273 **Description: Fourier analysis.** Color responses can be analyzed using Fourier analysis (Krauskopf et al.,
274 1982; Stoughton et al., 2012) that identifies the set of sine waves (frequency, phase angle, and
275 amplitude) that capture the shape of the color-tuning function. We extracted for each cell the
276 normalized amplitude and phase angle of the first 8 harmonics; most of the power was captured by the
277 first two harmonics. The first harmonic has a single peak when plotted in polar coordinates of color
278 space (i.e. a vector pointing to one color); the second harmonic identifies an axis in these coordinates
279 (i.e. the poles of the axis identify an opponent color pair). Confidence interval of the mean was obtained
280 by resampling cells with replacement and computing the angular mean 1000 times (for the second
281 harmonic, for all cells we used the peak between 0 and 180°).

282 *Correlation between fMRI and electrophysiology*
283 We correlated the single cell activity for each of the 16 hues for all single cells of all three monkeys
284 separately for each face patch, to the average percent signal change to these 16 hues obtained by
285 interpolating from the signal change to the 12 hues used in the fMRI experiment (face-patches were
286 identified over the 2 hemispheres of M1 and M2 of the current study, details of stimuli and ROI
287 definition can be found in Rosenthal et al., 2018). Note that in order to make the Bold response and
288 neurons' firing rate more comparable, we averaged the net firing rate over the entire window from
289 stimulus onset to the onset of the next stimulus (400 ms). The firing rate is thus lower than when
290 selecting a response window tailored to each cell.

291 *Population information*
292 To compute the population of face-selective cells' Fisher information, we fitted each cell's net average
293 firing rate response to the 16 hues by a von Mises function of the form $r(\theta) = a + b\exp(\kappa[\cos(\theta - $

7

294 θ_{pref})]]), with $\kappa > 0$, $a > 0$ and $b \geq 0$ (median Mean Squared Error across all cells of 0.38 spks/s). The
295 population Fisher information is given by:

$$I_F(\theta) = \left\langle \left(\frac{\partial \ln(p[\mathbf{r}|\theta])}{\partial \theta}\right)^2 \right\rangle$$

296 Assuming independent Poisson noise, we can derive that:

$$I_F(\theta) = \sum_{n=1}^{173} \frac{\left(f'_n(\theta)\right)^2}{f_n(\theta)}$$

297 Where f_n represents the tuning function for cell n.
298 For visualization, we also present the population information smoothed with a Savitsky-Golay filter
299 (window of 50 degrees, first order polynomial). We also computed the 95% confidence intervals of the
300 Fisher information using non-parametric bootstrapping with 1000 iterations.

301 Finally, we performed the same analysis with the original 16 CIELUV hue angles projected along the 2
302 chromatic axes: 180°-0° corresponding to greenish to reddish hues, and 270°-90° corresponding to
303 bluish to yellowish hues.

304 *Distribution of natural face color*
305 Xiao et al., 2017 measured the spectra of skin on the cheek, forehead, back of hand and inner arm of
306 960 participants of 4 ethnicities (Caucasian, Chinese, Kurdish and Thai) under D65 illuminant, and
307 reported the mean and standard deviation of the CIELAB values for each body part and each ethnicity in
308 CIELAB color space. We averaged the forehead and cheek L, a* and b* means and standard deviations
309 (Table 2). We then computed a weighted average across all ethnicities for both mean and standard
310 deviation (using Table 1). Using standard conversion matrices from CIELAB to XYZ and XYZ to CIELUV we
311 obtained an estimate of the mean and standard deviation of the distribution of face color in CIELUV hue
312 angle, represented as a von Mises distribution in Figure 11.

313 **Results**

314 Functional magnetic resonance imaging was used to identify regions of inferior temporal cortex that
315 were more responsive to faces than to bodies and fruits, a standard contrast used to identify face
316 patches (Tsao et al., 2006; Lafer-Sousa and Conway, 2013). We targeted microelectrodes to the ML face
317 patch in two monkeys (M1 and M2) and the AL face patch in three monkeys (M1, M2 and M3; **Figure
318 2A**). To screen for face-selective neurons, we measured the responses of each cell to a battery of
319 grayscale images of 14 categories (**Figure 2B**). Face-selective neurons, such as the two examples in
320 Figure 2B, were defined as those that showed at least a twofold greater response to faces than bodies
321 and fruits. This selection criterion yielded 102 single units in ML and 71 single units in AL. Face-selective
322 cells in AL had a higher face selectivity index than cells in ML (**Figure 2C**; Mdn_{ML} = 0.60, Mdn_{AL} = 0.92,
323 Mann-Whitney-Wilcoxon rank-sum test U=1842, *p*<0.001); cells in AL and ML had similar firing rates
324 (Mdn_{ML} = 6.38, Mdn_{AL} = 6.28, U=3671, *p*>0.88). All face-selective cells showed a significant main effect of
325 face image (repeated measures ANOVA on a cell-by-cell basis; responses were the average firing rate
326 during the response window to each face images; analysis restricted to the 102 neurons that were
327 tested with at least three presentations of each face image; all neurons were p<0.05). The preferred
328 face was more likely a monkey face (70% of the cells), and more likely a 3/4 view than a front view (64%

329 of the cells). Across all cells, the preferred stimulus triggered a firing rate with a median 2.3 times higher
330 than when using the average we are using for all analyses (IQR: [1.7, 3.0]).

331 We next measured responses to color for the face-selective neurons. Color responses were obtained
332 using monochromatic versions of photographs of faces, bodies, and fruits (**Figure 3A**); the colored
333 stimuli evenly sampled CIELUV color space (**Figure 3B**, top panel). We chose to define the stimuli in
334 CIELUV color space because this space captures the representation of color within the V4 Complex
335 (Bohon et al., 2016), which provides input into inferior temporal cortex (Kravitz et al., 2012). The
336 chromaticity of the stimuli can be transformed into cone-opponent "DKL" space, which reflects the
337 cone-opponent cardinal mechanisms evident in the lateral geniculate nucleus (Derrington et al., 1984;
338 Sun et al., 2006) (**Figure 3B**, bottom panel). Evaluating color responses in DKL space is useful because it
339 has a physiological basis; throughout the paper, the CIE colors corresponding to the poles of the cone-
340 opponent axes (L>M, M>L, S+, and S-) are provided to facilitate this evaluation. To create a given image
341 in a target color, we replaced each pixel in the original gray-scale image with the target hue of the same
342 luminance value as the pixel. Thus the false-colored images maintained the luminance contrast of the
343 original image.

344 **Figure 4** shows the responses of a representative sample of six face-selective neurons to the colored
345 images of faces, bodies, and fruit; cells 1-3 were recorded in face patch ML; cells 4-6 were recorded in
346 face patch AL. The top panels show the average responses to images of faces, bodies, and fruits. As
347 predicted given the screening criterion, responses were always substantially larger to faces than to the
348 other stimulus categories, with face-selectivity indices ranging from 0.44 to ~1. For each cell we defined
349 a time period for quantification of the responses (blue bar in **Figure 4A, 3B**). We used a single
350 continuous time period for all cells whose duration was tailored to each cell. The response of cells
351 showed complex temporal dynamics. For example, cell #4 showed two peaks (at 105 ms and 225 ms)
352 and the intervening firing rate dipped back to baseline—in cells such as this one, the time period for
353 quantification only included the initial peak. Using multiple time periods for some cells such as cell #4
354 did not change the main conclusions (data not shown). The median latencies and the duration of the
355 response time periods across the population of cells are reported in **Table 1**. Cells in ML showed a
356 shorter latency than cells in AL within each monkey. But the variability in latencies for cells in ML or AL
357 across monkeys was greater than the difference in latency between ML and AL within any monkey.

358 The top panels in **Figure 4B** show post-stimulus-time-histograms (PSTHs) of the responses to the colored
359 faces, averaging across the four different face categories we used (monkey and human faces, frontal
360 faces and ¾-view faces; see Figure 2B). The orientation of the PSTH shows time on the y-axis and image
361 color on the x-axis. The stimulus onset is at 0 seconds, and darker gray corresponds to higher firing rate.
362 The responses of the neurons are delayed by a latency reflecting the time for visual signals to be
363 processed by the retina and relayed through the visual-processing hierarchy to inferior temporal cortex.
364 The cells in **Figure 4** were representative of the population: three of the cells were modulated by the
365 color of the stimulus (cells #1, #3, #6), reflected in the average response over the response window
366 (black trace below the PSTH; see methods for significance calculation). Among the population of face-
367 selective neurons, ~25% were significantly modulated by color (23/102 cells in ML; 21/71 cells in AL).
368 Cells #2, #4, and #5 were not modulated significantly by color. The red traces in Figure 4B show the best-
369 fitting sine wave following Fourier analysis of the color responses, described below.

9

370 Note that the firing rates shown in the bottom panels of **Figure 4B** are averages over the response
371 window and so are lower than the peak firing rates shown in **Figure 4A**. Although many cells were
372 modulated by color, the variance in firing rate caused by changes in color was modest. For example, the
373 firing rate in cell #3 varied between 18 and 22 spikes/second above background, which corresponds to
374 +/- 10% of the average stimulus-driven response. Across the population, the variation in firing rate due
375 to hue was +/-24% of the average stimulus-driven response. About 76% of the stimulus-driven response
376 can be therefore attributed to the luminance contrast of the images.

377 **Figure 4C** plots the cells' responses as a function of color angle; the norm of the vector sum is shown as
378 the bolded black line, and varies between 0 and 1 (0=equal net firing rate for all hues identical, i.e. no
379 color tuning; values for each cell are shown in black text). To further quantify the results, we determined
380 the best-fitting sine wave of the color-tuning response for each cell (red lines, **Figure 4B**). Many cells
381 (71/173) were best fit by the first harmonic (a single cycle), which shows that these cells have a single
382 preferred color (see cell #3, #6, **Figure 4**); but some cells were best fit by the second harmonic (21/173),
383 indicative of a preference for a color axis in color space, rather than a single color direction (cell #1,
384 **Figure 4**). The amplitude and phase angle of the best fitting harmonic is shown in red in **Figure 4C**. The
385 color preferences assessed by the norm of the vector sum and the normalized amplitude of the first
386 harmonic were highly correlated (Pearson r=0.93, p<0.001). Among the 44 cells showing significant color
387 modulation, the power of both the first and the second harmonic was higher than the noise level
388 estimated as the power to the 8th harmonic (red lines, **Figure 5**); 37/44 cells showed highest power to
389 the first harmonic; 5/44 showed highest power to the second harmonic; 1/44, to the third; and 1/44 to
390 the fourth. We found no evidence that the color selectivity of the cells depended on the cells' face
391 preference: for each neuron, we computed the color selectivity (as the normalized amplitude of the first
392 Fourier component) for each face image. We then rank-ordered the face images by descending average
393 firing rate and ran a repeated measures ANOVA with the ranks as independent variables. There was no-
394 significant main effect of the rank on color selectivity (p > 0.13).

395 Figure 4 provide evidence that some face-selective cells were sensitive to color. Among the population,
396 was there a consistent color preference? **Figure 6** shows the color responses of all the face-selective
397 cells rank-ordered by the significance of the color tuning, with the most significantly color-tuned cells at
398 the top. Each row shows data from one cell. The gray level shows the normalized response to the given
399 color (the sum of the values across colors for a given cell is 1). Many of the most significantly color-
400 tuned neurons in both ML and AL preferred warm colors, as evident by the dark regions on the upper
401 left and right of the panels in Figure 6. But there were some exceptions. For example, cells represented
402 by rows 6 and 7 in the ML panel and rows 1 and 2 in the AL panel of Figure 6 showed a preference for
403 greenish colors.

404 **Figure 7** quantifies the color responses of the population of single cells using Fourier analysis. The left
405 panel of Figure 7A shows a polar histogram of the peak color direction for cells with maximum power to
406 the first harmonic; significantly color-tuned cells are shown in dark gray. These results confirm the
407 population bias towards the red pole of the 0°-180° chromatic axis, corresponding to the L>M pole of
408 the L-M cone-opponent axis. This bias is also evident when analyzing the color direction of the best-
409 fitting first harmonic for all cells in the population (including those that did not have maximum power in
410 the first harmonic, **Figure 7B**, left panel). In contrast, cells with maximum power to the second harmonic
411 showed a phase angle biased for the 90°-270° axis, corresponding to modulation along the S-cone axis
412 (**Figure 7A**, right panel). And this bias was also evident when analyzing the best fitting second harmonic

413 for all cells in the population (including those that did not have maximum power in the second
414 harmonic; **Figure 7B**, right panel). The pattern of results shown in Figure 7 was evident when analyzing
415 data for each animal separately (**Figure 7C**).

416 How does color tuning relate to color selectivity? If color tuning reflects a computational operation of
417 the circuit one might predict that within the population more color-selective cells will have more
418 consistent color tuning. **Figure 8** quantifies the polar direction of the norm of the vector average (i.e. the
419 peak color preference; y-axis), color selectivity (x-axis), significance of color tuning (symbol gray value),
420 and number of stimulus repeats obtained (symbol size). The data points to the right of the plot
421 converge on 0 degrees (the L>M pole of the L-M axis), consistent with the prediction. Significantly color-
422 tuned neurons, defined by the p<0.05 threshold had a mean preferred hue angle that did not differ from
423 insignificantly color-tuned neurons (Watson-Williams test, F(1, 171)=0.07, p=0.80) but had a
424 significantly lower variance (**Figure 8**, marginal distribution, Wallraff test, χ^2=11.59, p<0.001). This effect
425 cannot be attributed to variance in the amount of data collected for different neurons. Indeed, splitting
426 the population into two groups, above and below the median number of trials collected per cell, yielded
427 a similar variance in the peak color for two groups (Wallraff test, χ^2=1.10, p=0.29).

428 The face-selective neurons responded strongly to all the colored stimuli, even those of suboptimal color
429 (see Figure 4). We attribute the strong color-independent responses to the luminance contrast of the
430 stimuli (regardless of the color, the stimuli preserved the luminance contrast of the original images). We
431 can directly dissect the role of color and luminance contrast on the cell responses by using equiluminant
432 colored stimuli (**Figure 9A**). These stimuli were created by replacing the range of gray values in the
433 original images with colors of a constant gray value but different saturation: higher luminance gray
434 values were replaced with more saturated color. Responses to these equiluminant stimuli were
435 substantially lower than responses to the colored stimuli that preserved luminance contrast (**Figure 9B**;
436 Mdn_{Iso} = 0.99, Mdn_{Main} = 7.64, Wilcoxon rank-sum test U=4643, p<0.001). These results show that pure
437 color is not sufficient to strongly drive face-selective cells. Because there is no accepted metric for
438 relating color contrast and luminance contrast (Shevell & Kingdom, 2008), it is often difficult to compare
439 responses to equiluminant stimuli with responses to luminance contrast stimuli. In the present study,
440 this difficulty is mitigated for several reasons. First, the maximum color contrast of the equiluminant
441 stimuli was the highest that the gamut of the display could produce. If color were a sufficient drive of
442 the neural activity of face-selective neurons, the equiluminant stimuli we used should elicit strong
443 responses. Second, using stimuli of comparable color and luminance contrast, other neurons in the
444 visual system show clear preferences for the color stimuli (in V1: Conway, 2001, Horwitz and Hass, 2012,
445 Johnson et al, 2004; in V4, Conway et al, 2007, Bohon et al, 2016; in IT, Komatsu 1998; Lafer-Sousa and
446 Conway, 2013), confirming that these stimuli are capable of eliciting strong responses when neurons are
447 responsive to color.

448 We previously measured the color responses across IT using fMRI (Lafer-Sousa and Conway, 2013;
449 Rosenthal et al., 2018). To directly compare the results of the fMRI with the cell data, we quantified the
450 neural responses within a 400 ms time window starting at the stimulus onset. This time window
451 encompasses the 200 ms duration of the stimulus and the 200 ms inter-stimulus gray period. **Figure 10A**
452 shows the average response for the population, in ML (solid line) and AL (dotted line). The plot shows
453 significant differences among the responses to the colors (non-parametric Friedman test, χ^2= 210.69,
454 p<0.001) and the responses in ML are highly correlated with those in AL (Pearson r=0.89, p<0.001).
455 **Figure 10B** shows the average response across all face-selective cells to face images in each of the 16

11

456 colors. This plot underscores two main conclusions: first, responses to all colored images were strong,
457 which we attribute to the fact that all the colored exemplars preserved the luminance contrast of the
458 original achromatic images—the luminance contrast is a main determinant of face-selective responses
459 (Ohayon et al., 2012); and second, among the colored stimuli, responses to the L>M stimuli (appearing
460 pinkish) were higher than response to the M<L stimuli (appearing greenish). The color biases of the
461 population of face-selective cells was strongly correlated with the color biases of the face patches
462 measured with fMRI (**Figure 10C**, ML: Pearson r=0.67, p=0.005, power=0.84; AL: Pearson r=0.61 p=0.01,
463 power=0.75).

464 The data presented above quantify the color-tuning properties of face cells. If the color responses of
465 face-selective cells reflect a role these cells play in discriminating face colors, we predicted that the
466 Fisher information of the population would correspond to the distribution of face colors. The color
467 statistics of face skin are available in a large data base of calibrated measurements derived from
468 multiple ethnicities (Xiao et al., 2017). We assume that the color statistics of bare macaque face skin
469 shows a comparable bias to that found across humans (and we assume that neural measurements in
470 macaque monkeys extend to the human case). **Figure 11 C** shows the Fisher information computed for
471 the neural data as a function of hue angle using von Mises function to describe the cells' response
472 (**Figure 11 A**). Superimposed on the panels is the distribution of face colors (dashed curves). The peak of
473 the distribution of face colors does not correspond to maxima in the Fisher information; to the contrary,
474 the likely colors of faces corresponds to a dip in the Fisher information, which implies that the
475 population is poor at discriminating the colors of faces. We did the same analysis projecting the original
476 data along the 0-180 deg axis in CIELUV space, which approximates the L-M axis (**Figure 11 B, C,** middle
477 panels), to evaluate whether face cells contain more information about the color component of faces
478 that is most relevant for dynamic social signaling (the red pole of the green-red axis) (Hasantash et al.,
479 2019). In this analysis, the Fisher information peaks for reddish colors, consistent with the idea that face
480 cells are color-tuned in a way that can contribute to the discrimination of L>M values. For comparison,
481 the right panels **of Figure 11 B, C** show the analysis for data along the vertical axis in CIE color space,
482 which approximates the S-cone axis. Face-selective cells did not show selective tuning along the S-cone
483 axis; the Fisher information analysis implies that the cells do not carry as much information along the S-
484 cone axis as they do along the L-M axis.

485

486 **Discussion**

487 The population of face-selective neurons showed broad color tuning with a bias for reddish colors. The
488 Fisher information, which reflects how well the neural population can discriminate among colors, shows
489 a dip which coincides with the peak in the distribution of face colors measured across human ethnicities
490 (Xiao et al., 2017). This pattern of results implies that face-selective cells in macaque IT are not optimally
491 tuned to discriminate the colors of human faces. It is conceivable that face-selective neurons in
492 macaque IT are optimally tuned to discriminate macaque face colors, although this would require a
493 substantial difference in the colors of macaque faces compared to human faces, which is unlikely since
494 the primary determinants of face coloring (oxygenated hemoglobin and melanin) are the same in both
495 species. It is also conceivable that the color responses of the neurons may be stronger if color was
496 manipulated in spatial patterns on the face to reflect the spatial distribution of natural color changes
497 over the face. Thus, the color responses we report provide a lower bound. The color tuning curves were

498 measured using images that preserve the normal luminance contrast relationships of face photographs.
499 In a second series of experiments, we found that face-selective cells were not very responsive to pure
500 color (equiluminant) images of faces, which underscores the importance of luminance contrast for face
501 selectivity (Ohayon et al., 2012), and provides single-unit evidence supporting the fMRI observation that
502 face patches respond more strongly to luminance contrast compared to equiluminant color (Lafer-Sousa
503 and Conway, 2013). Taken together with prior work, the research supports the idea that color-specific
504 information related to the discrimination of face colors is likely handled by neural circuits that are
505 independent of face patches. This interpretation is consistent with the multi-stage parallel processing
506 framework of inferior temporal cortex, in which face-biased regions are largely non-overlapping with
507 color-biased regions (Conway, 2018).

508 We related the neurophysiology results to behavior using an information framework. Optimal neural
509 coding suggests that there should be a good match between neural tuning and the statistics of those
510 parts of the environment that are relevant (Simoncelli and Olshausen, 2001; Ganguli and Simoncelli,
511 2010). Faces occupy a distinct gamut in color space (Crichton et al., 2012; Chauhan et al., 2015; Xiao et
512 al., 2017). If face-selective cells participate in discriminating among the colors of faces, the Fisher
513 information of the population of neural responses should correspond to the distribution of face colors.
514 The neurophysiological results refute this prediction. Most of the significantly color-tuned face-selective
515 neurons cells were best described as having broad tuning, with a single peak in the color-tuning
516 function. On average, the color-tuning peaks across cells were to warm (L>M) colors (**Figure 7**),
517 corresponding to the typical colors of faces. The Fisher information curve is bimodal and the color-
518 discrimination potential of face-selective neurons is therefore worse for face colors compared to greens
519 and purples (**Figure 11,** peaks at 84 and -66 hue angle).

520 These results suggest that some other population of neurons is responsible for discriminating the colors
521 of faces. Functional MRI response patterns in both macaque monkeys and humans show a multi-stage
522 organizational scheme governed by a repeated eccentricity template, in which color-biased tissue is
523 sandwiched between face-selective tissue (foveal biased) and place-selective tissue (peripheral biased)
524 in parallel streams along the length of the ventral visual pathway (Lafer-Sousa and Conway, 2013; Lafer-
525 Sousa et al., 2016; Conway, 2018). This organization provides the possibility that color-specific
526 information about objects, including faces, could be extracted by neural circuits besides the face
527 patches. But we note that within the face-selective population we studied, some cells were color-tuned
528 with peak tuning away from reddish colors; these cells were, curiously, the most color selective in the
529 population (top rows in **Figure 6**). These neurons may represent a distinct category of face-selective cells
530 that could, conceivably, be optimally tuned to discriminate the colors of faces.

531 What role, if any, does the color tuning of face cells play in visual processing? We consider three
532 possibilities. First, the information content with regards to color was not zero, so the cells could
533 discriminate face colors, but non-optimally. Second, the color component of faces to which humans are
534 most sensitive, regardless of race, is the aspect that varies in response to changes in emotion and
535 health, which is encoded selectively along the L-M chromatic axis (Hasantash et al., 2019). Could the
536 color tuning of face-selective neurons optimally discriminate just this component? Consistent with this
537 possibility, we found that the average tuning and the Fisher information increased for stimuli with larger
538 L>M values. The pattern of results is similar to the ramp-tuning functions of face-selective neurons for
539 other stimulus features (Freiwald et al., 2009). Thus the selectivity we observed implies that the extent
540 of L-M color contrast in a face is a relevant feature encoded by face-selective neurons. Finally, we

13

541   wonder if the color tuning may serve to enhance the face-discrimination computations of the neurons.
542   On average, faces have a warmer coloring than backgrounds (Rosenthal et al., 2018). It is plausible that
543   the color responses would increase the firing rates of face-selective neurons when a face is
544   encountered. Such modulation would presumably promote the role of these neurons in face
545   recognition. According to this interpretation, the modulation by color of face-selective cells is analogous
546   to the modulation of neural activity manifest when a subject engages in an attentional task (Wurtz and
547   Mohler, 1976; Treue, 2001; Maunsell, 2015).

548   Is the color tuning we describe specific for faces? Quantitative analysis of the color statistics of those
549   parts of scenes that we label, shows that objects tend to be systematically biased compared to
550   backgrounds: objects, not just faces, tend to be distinguished from backgrounds along the u' direction of
551   color space, which corresponds, roughly, to warm coloring (Gibson et al., 2017; Conway et al., 2019).
552   Tuning to warm coloring may therefore facilitate the computations of many cells in IT, not just face-
553   selective neurons. This hypothesis is supported by fMRI maps of the color tuning across IT, which show a
554   band running along the posterior-anterior axis that is more strongly modulated by the likely colors of
555   objects (Conway, 2018; Rosenthal et al., 2018). This band is centered on the face patches but is not
556   restricted to them. Consistent with the fMRI results, we found that the non-face-selective cells, often
557   found on the margins or just outside of face patches, also showed a weak bias for warm colors (**Figure**
558   **12**). Moreover, others have reported that the optimal stimuli for IT cells are often of warm coloring
559   (Ponce et al., 2019). We speculate that the modulation by color is likely not a specific property of face
560   cells but may reflect a feature of IT that facilitates the computation by IT of object recognition generally.

561   Although most cells had a single peak in the color-tuning function, some face-selective neurons were
562   best fit by two peaks, with maximum power to the second harmonic in the Fourier analysis (**see**
563   **example cell #1, Figure 4**). The color selectivity of this subset of neurons, assessed as the phase angle of
564   the second harmonic, was aligned with the S-cone axis in color space (**Figure 7**). Is the tuning to the
565   second harmonic meaningful? One possible concern could have been that these responses reflect a
566   luminance artifact: estimates of equiluminance may not be accurate, especially for colors that modulate
567   S cones (Vos, 1978). We avoided this potential pitfall in the present work because the stimuli preserved
568   the luminance contrast of the original images: the blackest and whitest regions in the colored versions
569   of each image were the same as in the original image. Any luminance artifacts attributed to vagaries in
570   the determination of equiluminance would be masked by preservation of the luminance contrast of the
571   original image.

572   The response bias to colors along the S axis was surprising; we think the results provide the first
573   measurements of color tuning biases within extrastriate cortex that reflect the cardinal mechanisms.
574   The cardinal mechanisms correspond to the color tuning of the cone-opponent cells that represent the
575   first post-receptoral stage of color encoding and are reflected in the anatomy and physiology of the
576   lateral geniculate nucleus (Derrington et al., 1984; Martin et al., 2001; Sun et al., 2006; Roy et al., 2009).
577   The cardinal mechanisms are evident in behavioral work that is thought to isolate these subcortical
578   contributions to color vision (Krauskopf et al., 1982; Eskew, 2009). The observation that cortical cells
579   reflect the cardinal mechanisms is surprising because the distinct chromatic signatures associated with
580   the cardinal mechanisms diffuse near the input layers to primary visual cortex (Tailby et al., 2008), and
581   the organization of color undergoes progressively more uniform representation of color space through
582   the visual-processing hierarchy (Bohon et al, 2016; Liu et al, 2020). The present results show that
583   chromatic signatures corresponding to the cardinal mechanisms reemerge in extrastriate cortical circuits
584   far along the putative visual-processing hierarchy, and they raise the possibility that the behavioral

585   results reflecting the cardinal mechanisms may derive from responses not only of subcortical circuits,
586   but also of extrastriate circuits.
587

588   **References**

589   Bohon KS, Hermann KL, Hansen T, Conway BR (2016) Representation of Perceptual Color Space in
590   Macaque Posterior Inferior Temporal Cortex (the V4 Complex). eNeuro 3.
591   Changizi MA, Zhang Q, Shimojo S (2006) Bare skin, blood and the evolution of primate colour vision. Biol
592   Lett 2:217-221.
593   Chauhan T, Xiao K, Yates J, Wuerger S (2015) Estimating discrimination ellipsoids for skin images. Journal
594   of Vision 15:820.
595   Conway BR (2009) Color vision, cones, and color-coding in the cortex. Neuroscientist 15:274-290.
596   Conway BR (2018) The Organization and Operation of Inferior Temporal Cortex. Annu Rev Vis Sci 4:381-
597   402.
598   Conway BR, Moeller S, Tsao DY (2007) Specialized color modules in macaque extrastriate cortex. Neuron
599   56:560-573.
600   Conway BR, Ratnasingam S, Jara-Ettinger J, Futrell R, Gibson E (2019) Communication efficiency of color
601   naming across languages provides a new framework for the evolution of color terms. Cognition
602   in press.
603   Crichton S, Pichat J, Mackiewicz M, Tian G, Hurlbert AC (2012) Skin chromaticity gamuts for illumination
604   recovery. Society for Imaging Science and Technology, Conference on Color in Graphics,
605   Imaging, and Vision, Amsterdam, the Netherlands:266-271.
606   Derrington AM, Krauskopf J, Lennie P (1984) Chromatic mechanisms in lateral geniculate nucleus of
607   macaque. Journal of Physiology 357:241-265.
608   Edwards R, Xiao D, Keysers C, Foldiak P, Perrett D (2003) Color sensitivity of cells responsive to complex
609   stimuli in the temporal cortex. J Neurophysiol 90:1245-1256.
610   Eskew RT, Jr. (2009) Higher order color mechanisms: a critical review. Vision Res 49:2686-2704.
611   Freiwald WA, Tsao DY, Livingstone MS (2009) A face feature space in the macaque temporal lobe. Nat
612   Neurosci 12:1187-1196.
613   Ganguli D, Simoncelli EP (2010) Implicit encoding of prior probabilities in optimal neural populations.
614   Adv Neural Inf Process Syst 2010:658-666.
615   Gerald MS, Waitt C, Little AC (2009) Pregnancy coloration in macaques may act as a warning signal to
616   reduce antagonism by conspecifics. Behav Processes 80:7-11.
617   Gibson E, Futrell R, Jara-Ettinger J, Mahowald K, Bergen L, Ratnasingam S, Gibson M, Piantadosi ST,
618   Conway BR (2017) Color naming across languages reflects color use. P Natl Acad Sci USA
619   114:10785-10790.
620   Golz J, MacLeod DI (2002) Influence of scene statistics on colour constancy. Nature 415:637-640.
621   Hasantash M, Lafer-Sousa R, Afraz A, Conway BR (2019) Paradoxical impact of memory on color
622   appearance of faces. Nat Commun 10:3010.
623   Kanwisher N, McDermott J, Chun MM (1997) The fusiform face area: a module in human extrastriate
624   cortex specialized for face perception. J Neurosci 17:4302-4311.
625   Kemp R, Pike G, White P, Musselman A (1996) Perception and recognition of normal and negative faces:
626   the role of shape from shading and pigmentation cues. Perception 25:37-52.
627   Komatsu H, Ideura Y (1993) Relationships between color, shape, and pattern selectivities of neurons in
628   the inferior temporal cortex of the monkey. J Neurophysiol 70:677-694.
629   Krauskopf J, Williams DR, Heeley DW (1982) Cardinal directions of color space. Vision Research 22:1123-
630   1131.
631   Kravitz DJ, Saleem KS, Baker CI, Ungerleider LG, Mishkin M (2012) The ventral visual pathway: an
632   expanded neural framework for the processing of object quality. Trends Cogn Sci 17:26-49.
633   Lafer-Sousa R, Conway BR (2013) Parallel, multi-stage processing of colors, faces and shapes in macaque
634   inferior temporal cortex. Nat Neurosci 16:1870-1878.

635   Lafer-Sousa R, Conway BR, Kanwisher NG (2016) Color-Biased Regions of the Ventral Visual Pathway Lie
636   between Face- and Place-Selective Regions in Humans, as in Macaques. J Neurosci 36:1682-
637   1697.
638   Lefevre CE, Ewbank MP, Calder AJ, von dem Hagen E, Perrett DI (2013) It is all in the face: carotenoid
639   skin coloration loses attractiveness outside the face. Biol Lett 9:20130633.
640   Leopold DA, Rhodes G (2010) A comparative view of face perception. J Comp Psychol 124:233-251.
641   Liu, Y., Li, M., Zhang, X., Lu, Y., Gong, H., Yin, J., ... & Shipp, S. (2020). Hierarchical Representation
642   for Chromatic Processing across Macaque V1, V2, and V4. Neuron. S0896-6273.
643   Martin PR, Lee BB, White AJ, Solomon SG, Ruttiger L (2001) Chromatic sensitivity of ganglion cells in the
644   peripheral primate retina. Nature 410:933-936.
645   Maunsell JHR (2015) Neuronal Mechanisms of Visual Attention. Annu Rev Vis Sci 1:373-391.
646   Nakajima K, Minami T, Nakauchi S (2017) Interaction between facial expression and color. Sci Rep
647   7:41019.
648   Nestor A, Tarr MJ (2008) Gender recognition of human faces using color. Psychol Sci 19:1242-1246.
649   Ohayon S, Freiwald WA, Tsao DY (2012) What makes a cell face selective? The importance of contrast.
650   Neuron 74:567-581.
651   Perrett DI, Rolls ET, Caan W (1982) Visual neurones responsive to faces in the monkey temporal cortex.
652   Exp Brain Res 47:329-342.
653   Petersdorf M, Dubuc C, Georgiev AV, Winters S, Higham JP (2017) Is male rhesus macaque facial
654   coloration under intrasexual selection? Behav Ecol 28:1472-1481.
655   Ponce CR, Xiao W, Schade PF, Hartmann TS, Kreiman G, Livingstone MS (2019) Evolving Images for Visual
656   Neurons Using a Deep Generative Network Reveals Coding Principles and Neuronal Preferences.
657   Cell 177:999-1009 e1010.
658   Rosenthal I, Ratnasingam S, Haile T, Eastman S, Fuller-Deets J, Conway BR (2018) Color statistics of
659   objects, and color tuning of object cortex in macaque monkey. J Vis 18:1.
660   Roy S, Jayakumar J, Martin PR, Dreher B, Saalmann YB, Hu D, Vidyasagar TR (2009) Segregation of short-
661   wavelength-sensitive (S) cone signals in the macaque dorsal lateral geniculate nucleus. Eur J
662   Neurosci 30:1517-1526.
663   Setchell JM, Wickings EJ (2005) Dominance, status signals and coloration in male mandrills (Mandrillus
664   sphinx). Ethology 111:25-50.
665   Shevell, S. K., & Kingdom, F. A. (2008). Color in complex scenes. *Annu. Rev. Psychol.*, *59*, 143-166.
666   Simoncelli EP, Olshausen BA (2001) Natural image statistics and neural representation. Annu Rev
667   Neurosci 24:1193-1216.
668   Sinha P, Balas BJ, Ostrovsky Y, Russell R (2006) Face Recognition by Humans:Nineteen Results All
669   Computer Vision Researchers Should Know About. Proceedings of the IEEE 94:1948-1962.
670   Stoughton CM, Lafer-Sousa R, Gagin G, Conway BR (2012) Psychophysical chromatic mechanisms in
671   macaque monkey. J Neurosci 32:15216-15226.
672   Sun H, Smithson HE, Zaidi Q, Lee BB (2006) Specificity of cone inputs to macaque retinal ganglion cells. J
673   Neurophysiol 95:837-849.
674   Tailby C, Solomon SG, Dhruv NT, Lennie P (2008) Habituation reveals fundamental chromatic
675   mechanisms in striate cortex of macaque. J Neurosci 28:1131-1139.
676   Treue S (2001) Neural correlates of attention in primate visual cortex. Trends in neurosciences 24:295-
677   300.
678   Tsao DY, Freiwald WA, Tootell RB, Livingstone MS (2006) A cortical region consisting entirely of face-
679   selective cells. Science 311:670-674.
680   Vos JJ (1978) Colorimetric and photometric properties of a 2° fundamental observer. Color Res Appl
681   3:125-128.

682 Waitt C, Gerald MS, Little AC, Kraiselburd E (2006) Selective attention toward female secondary sexual
683   color in male rhesus macaques. Am J Primatol 68:738-744.
684 Webster MA, MacLeod DI (2011) Visual adaptation and face perception. Philos Trans R Soc Lond B Biol
685   Sci 366:1702-1725.
686 Wei XX, Stocker AA (2015) A Bayesian observer model constrained by efficient coding can explain 'anti-
687   Bayesian' percepts. Nat Neurosci 18:1509-1517.
688 Wurtz RH, Mohler CW (1976) Enhancement of visual responses in monkey striate cortex and frontal eye
689   fields. J Neurophysiol 39:766-772.
690 Xiao K, Yates JM, Zardawi F, Sueeprasan S, Liao N, Gill L, Li C, Wuerger S (2017) Characterising the
691   variations in ethnic skin colours: a new calibrated data base for human skin. Skin Res Technol
692   23:21-29.
693 Yamashita JA, Hardy JL, De Valois KK, Webster MA (2005) Stimulus selectivity of figural aftereffects for
694   faces. J Exp Psychol Hum Percept Perform 31:420-437.

695

696

697

698

Figure and Table legends

700

Figure 1. Simulated population of 50 cells responding to a circular variable and corresponding Fisher information. A population with von Mises tuning curves of width t', amplitude a', and distribution of peaks p' yields a Fisher information with one peak. Each of these three parameters can be individually adjusted to create a population with a different Fisher information. Uniformly increasing tuning width (t'') while holding a' and p' constant yields a two-peaked Fisher information. Independently adjusting the distribution of tuning curve amplitudes (a'') or the distribution of the peaks (p'') creates an asymmetric Fisher information.

Figure 2. FMRI-guided microelectrode recording of face-selective cells in macaque inferior temporal cortex. **A.** Sagittal MR Images with recording micro-electrodes; superimposed is shown the fMRI contrast maps of faces>bodies uncover the face patches (ML-M2 top; AL-M3 bottom). Electrodes appear black in the MRI images, and target the face patches. **B**. Post-stimulus time histogram for an example cell in ML (top) and AL (bottom) showing the responses to achromatic images used to identify face cells. The red line along the x-axis shows the stimulus duration. **C.** Histogram showing the face-selectivity index (FSI) for the population of face cells in ML (top) and AL (bottom); the dashed vertical line shows the mean FSI. All cells with an FSI>=1/3 were included in the analysis.

Figure 3. Stimuli used to measure the color responses of face-selective cells in macaque inferior temporal cortex. **A.** Color space illustrating the procedure for generating the colored images. Each colored image was generated by replacing the pixels in the original achromatic image with a given hue that preserved the luminance of original pixel.   **B.** Sixteen colored versions were generated; the chromaticity of the most saturated pixel in each version is shown in CIELUV (u^*, v^*; top panel) and cone-opponent color space (DKL, bottom panel).

Figure 4. Responses to color of six face-selective cells in macaque inferior temporal cortex (2 cells for each monkey M1: #2, 3 – M2: #1, 5 – M3: #4, 6). **A.** Average responses to images of faces, bodies, and fruits. The time period during which the responses were quantified in subsequent analyses is shown by the blue bar along the x-axis. **B.** Post-stimulus time histogram (top panels) showing the average responses to colored images of faces; blue bar along the time axis as in panel A. Average response to face images of each color (bottom), quantified during the time period indicated by the blue bar in A and B. Error bars show 95% confidence intervals; the red line shows the best fitting sine wave. **C.** Polar plot showing normalized responses to all hues; the sum of the responses to the 16 colors is normalized to equal 1. The bold black text states the norm of the vector sum. The red line shows the normalized amplitude and phase of the best fitting sine wave for neurons whose best fit was a first or second harmonic; the red text states the value of the normalized amplitude of the best-fitting sine. The small black lines on the edges of the circle show the cardinal axes of the cone-opponent color space.

Figure 5. Power spectrum of the Fourier analysis of the color-tuning responses of face-selective neurons in macaque inferior temporal cortex. Average normalized amplitude of each harmonic component for the population of 173 cells (in black) and for significantly color-tuned cells (in red). Surrounding shaded

737   areas show 95% confidence intervals. Dashed and dotted lines represent the averages for respectively

738   ML and AL and solid lines the average across both face patches.

739   **Figure 6.** Responses to face images in each of 16 colors, for each cell in the ML face patch (top) and the

740   AL face patch (bottom). Each row shows data for one cell. Cells are ordered from the top by descending

741   color selectivity (p-value indicated by the color scale). The plot shows normalized responses: the sum of

742   the responses to the 16 colors for each row adds up to one (darker gray indicates relatively stronger

743   responses).

744   **Figure 7.** Fourier analysis of the color responses of face-selective cells in macaque inferior temporal

745   cortex. **A.** Left panel shows the distribution of the phase angle of the first harmonic component for cells

746   with higher amplitude in the first harmonic than the second harmonic (126/173 cells; Mean: -4.40

747   degrees CI=[-17.0,+8.5]); the right panel shows the phase angle of the second harmonic component for

748   cells with higher amplitude in the second harmonic compared to the first harmonic (47/173 cells; Mean:

749   +102.7 degrees CI=[+94.5,+111.1]). **B.** Distribution of the phase angle for the whole population (173

750   cells) for the first harmonic (left panel; mean +13.3 degrees CI=[-0.1,+27.9]) and the second harmonic

751   (right panel; Mean: +99.6 degrees CI=[+94.2,+105.3]). The color space is CIELUV; black tick marks are

752   provided for the cardinal axes of the cone-opponent DKL color space (these are offset from the axes of

753   CIELUV by 6.7 degrees). **C.** Distribution of the phase angles of the two first Fourier components across all

754   cells for each monkey plotted separately.

755   **Figure 8.** Quantification of the color responses of face-selective cells. Preferred hue angle (direction of

756   the average vector) is plotted as a function of the strength of the color preference (norm of the average

757   vector). Each face-selective cell is represented by a dot. The symbol size corresponds to the median

758   number of stimulus presentations per hue. The gray value of the symbols reflects the significance of the

759   color modulation (p-value). The marginal distribution shows the normalized distribution of the preferred

760   hue for significantly (dark grey) and non-significantly (light grey) color-tuned cells.

761   **Figure 9.** Response to equiluminant stimuli. **A.** Illustration of the construction of an L>M colored image.

762   The range of gray values in the original image were replaced with colors defined by a vector along an

763   equiluminant plane in the color space: white pixels of the original image were rendered in a saturated

764   hue; black pixels were rendered in gray; and gray pixels were rendered in a hue of intermediate

765   saturation. **B.** Firing rate above background of a population of face-selective neurons to equiluminant

766   stimuli (x-axis) versus luminance-preserved colored stimuli (y-axis; N=71 cells), each dot represents one

767   cell.

768   **Figure 10.** Comparison of color tuning measured using microelectrode recording of single cells in face

769   patches and fMRI. **A.** Average above-background firing rate computed over a 400 ms time window that

770   begins with the stimulus onset (peak responses away from 0 can be accounted for by summing the first

771   two harmonics of the response). **B.** Average above-background response for all face-selective cells

772   (N=173) to face images in 16 colors (the color of the traces corresponds to the colors of the images, see

773   Figure 3). **C.** Correlation between average response across the population of single units and fMRI color

774   tuning assessed in the face patches of monkeys M1 and M2 (see Methods).

775   **Figure 11.** Analysis of the Information represented in the population. **A.** Parameters of the von Mises fits

776   over the 173 face-selective cells used to compute the population information. **B.** Average net firing rate

777   across the population. **C.** Population Fisher information (thin line), smoothed Fisher information (thick
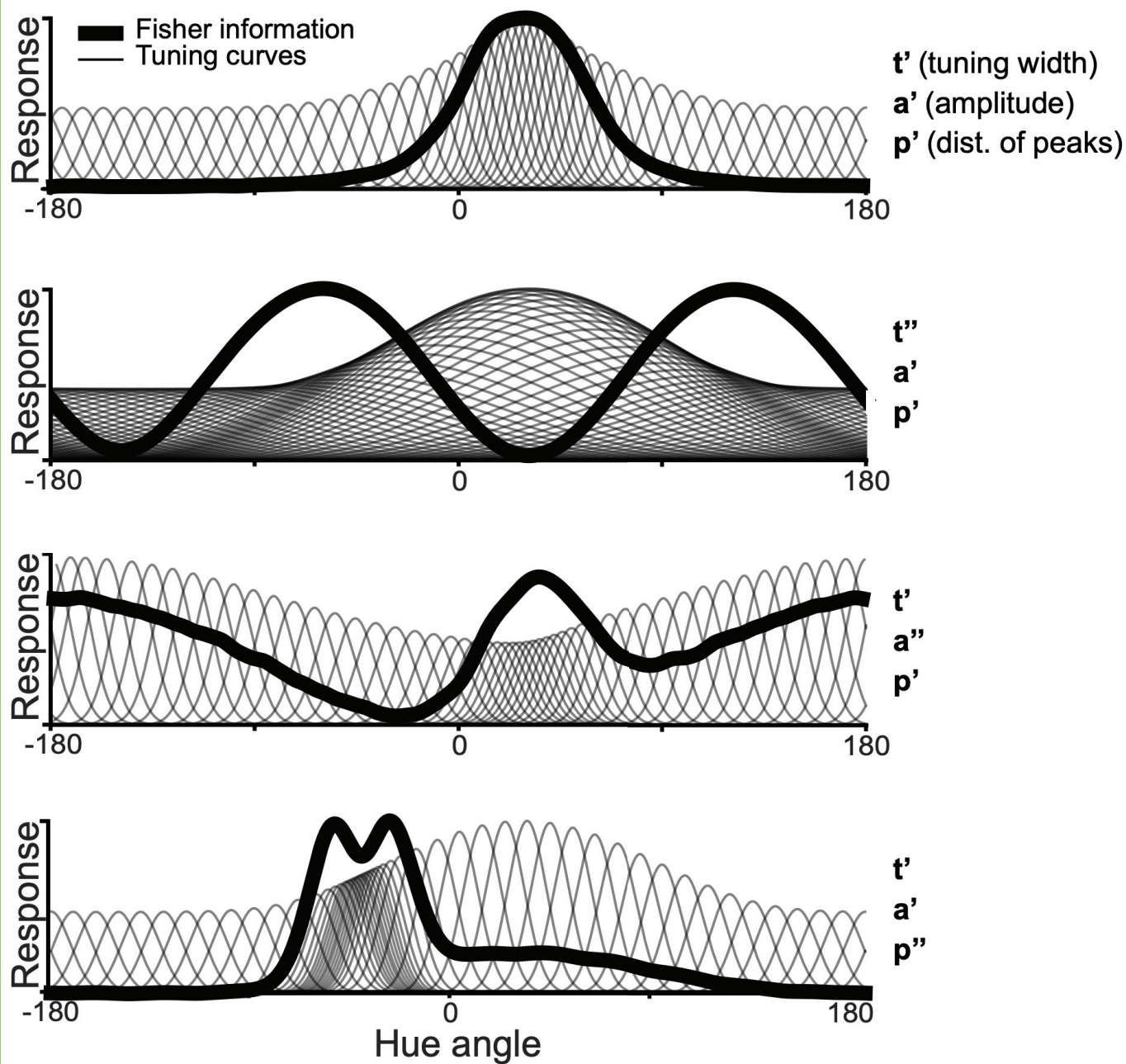
778   line) and 95% confidence intervals. On both panels, the dashed line represents the distribution of

779   natural face skin color, and the y-axis limits for Fisher information is kept constant across all 3 analyses.

780   The left column corresponds to the analysis performed in CIELUV space, the middle one to the analysis

781   projected along the greener to redder chromatic axis (positive values indicating redder), and the last one

782   to the analysis projected along the bluer to yellower chromatic axis (positive values indicating yellower).

783   **Figure 12.** Hue preference by Face Selectivity Index. Each dot represents one cell in one bin of 0.2.

784   Median and 95% confidence intervals on the median for each bin are represented above the kernel

785   density estimate of the distribution. The mean FSI across all 234 cells is 0.55.

786   **Table 1.** Number of cells, median latency and duration (in ms) of the response window used for the main

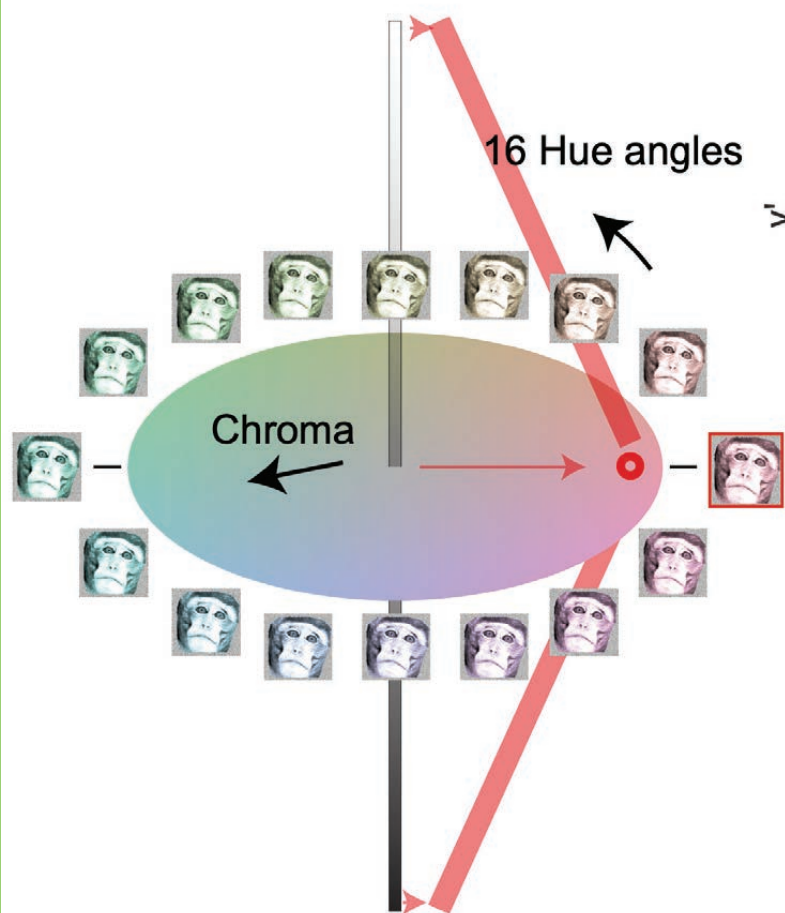787   analysis, by monkey and by face patch.

788   **Table 2** Coordinates of the target hues and adaptation point in Cie xyY, CIE LUV and cone contrast
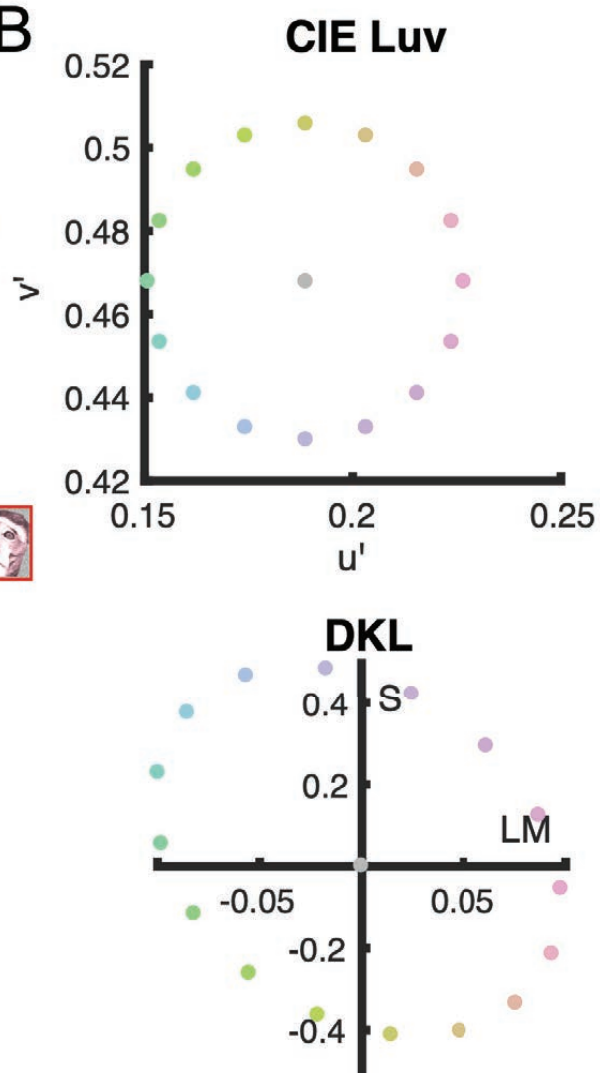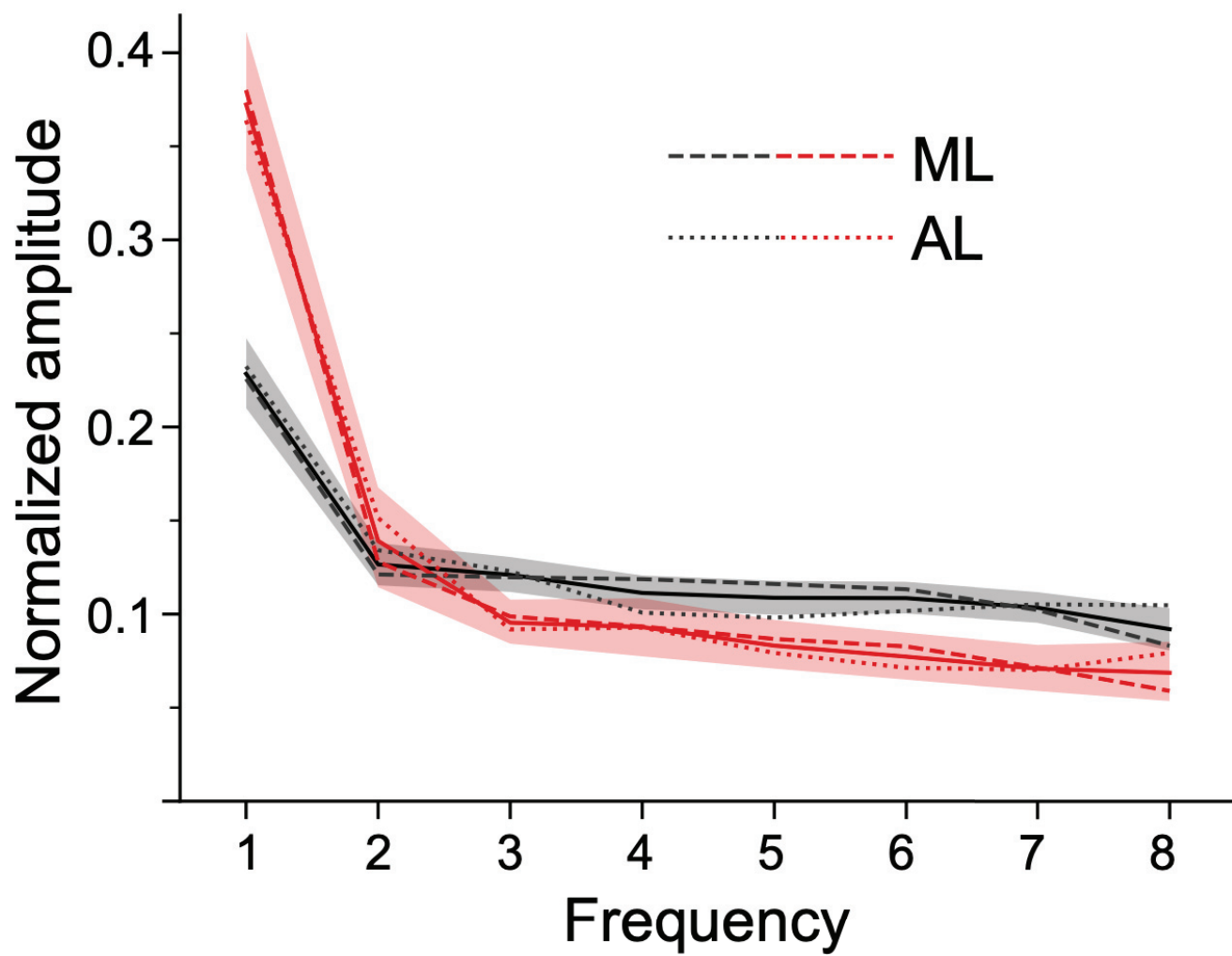
789   spaces.

790

Fisher information
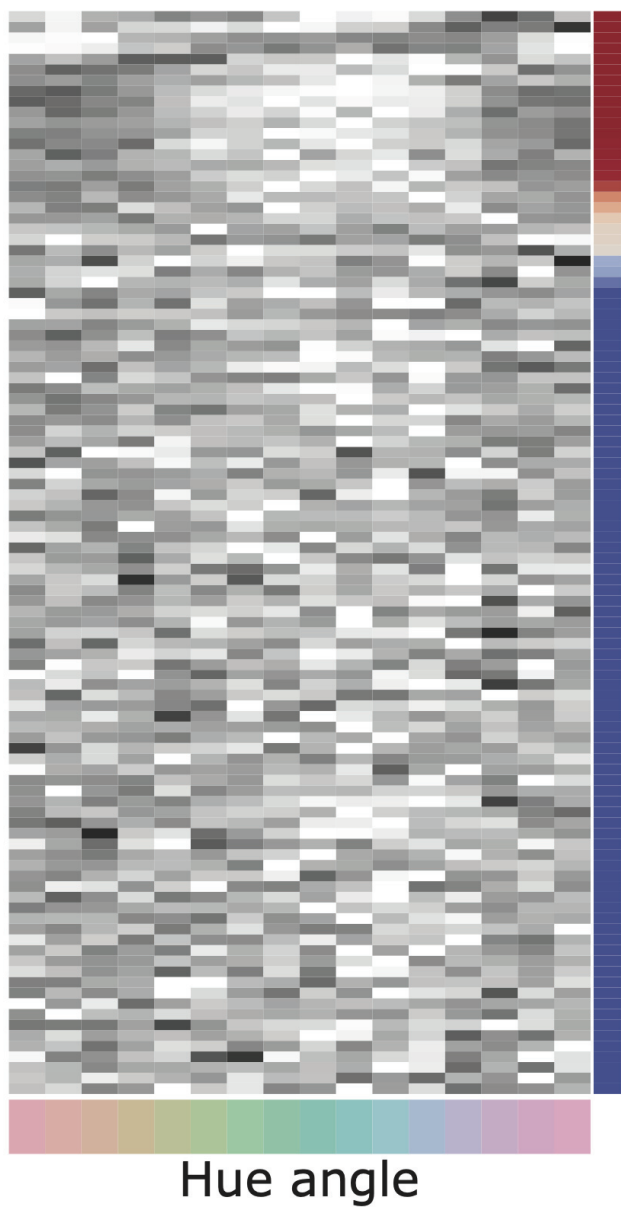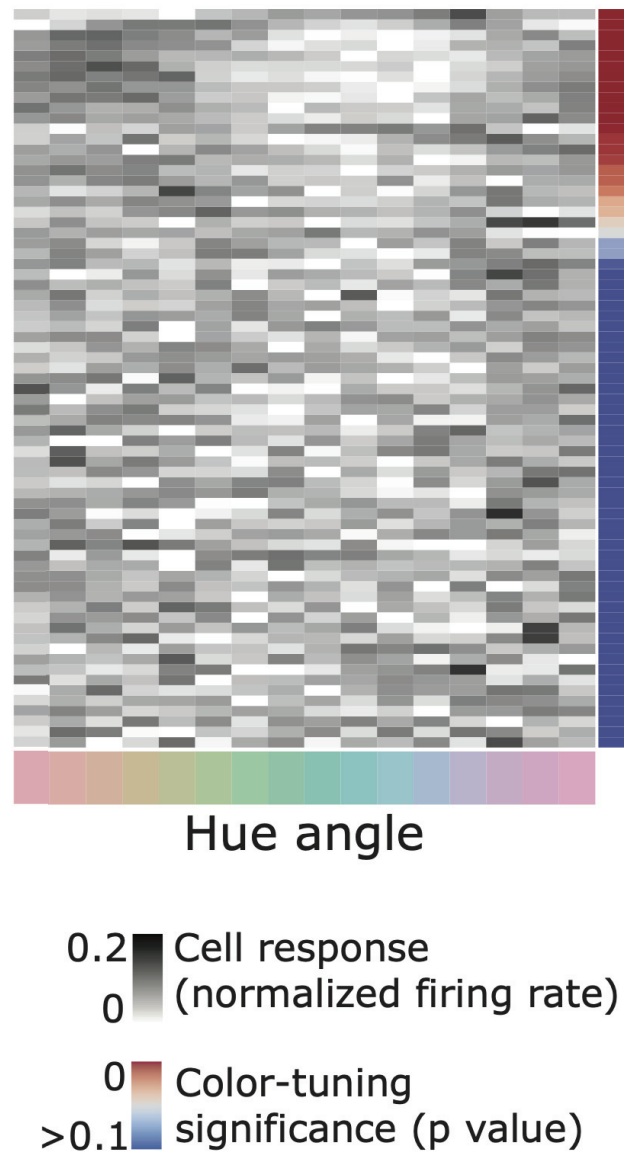Tuning curves

Response

-180   0   180

t' (tuning width)
a' (amplitude)
p' (dist. of peaks)

Response

-180   0   180

t"
a'
p'

Response

-180   0   180

t'
a"
p'

Response

-180   0   180

t'
a'
p"

Hue angle

A

16 Hue angles

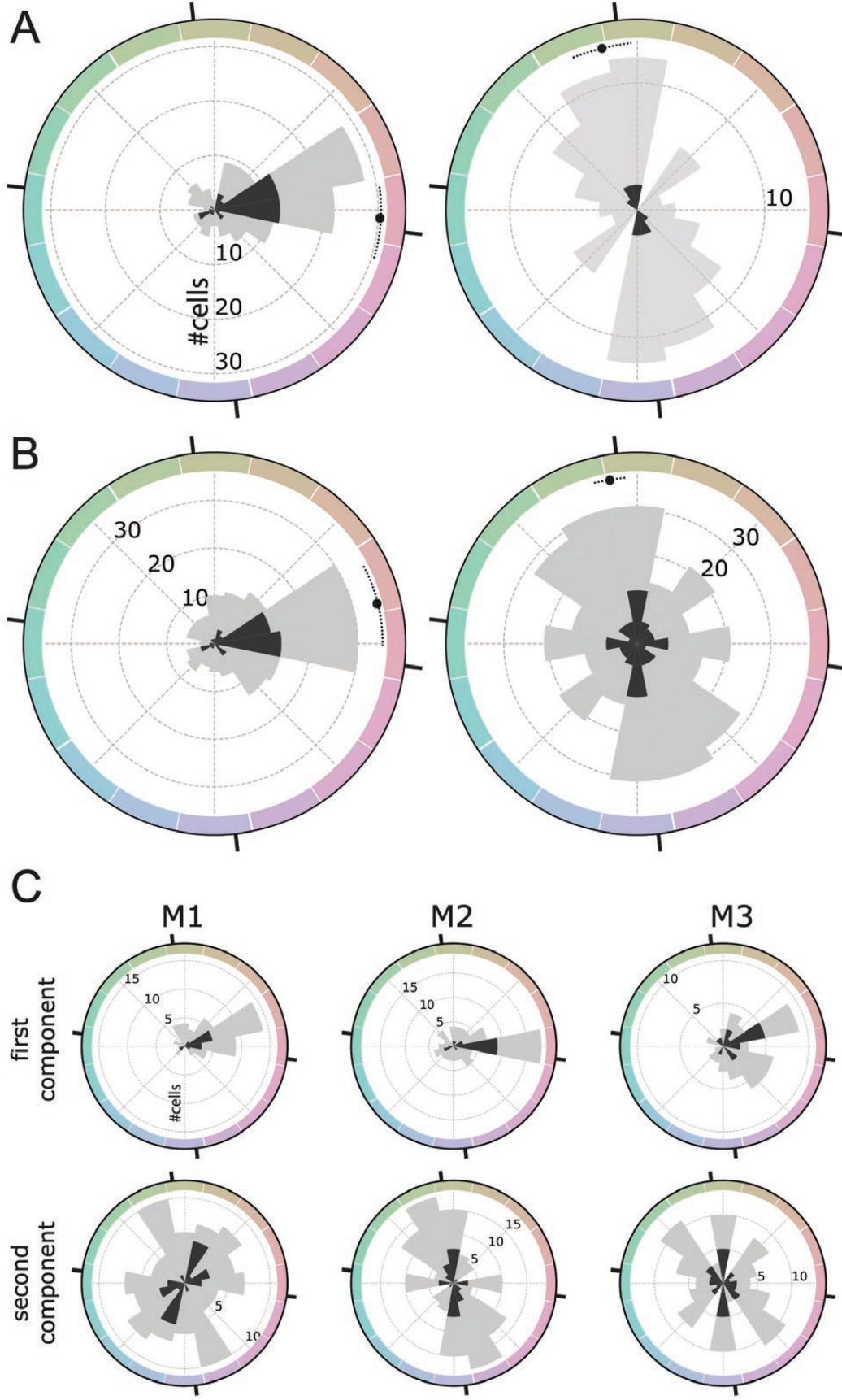Chroma

B **CIE Luv**
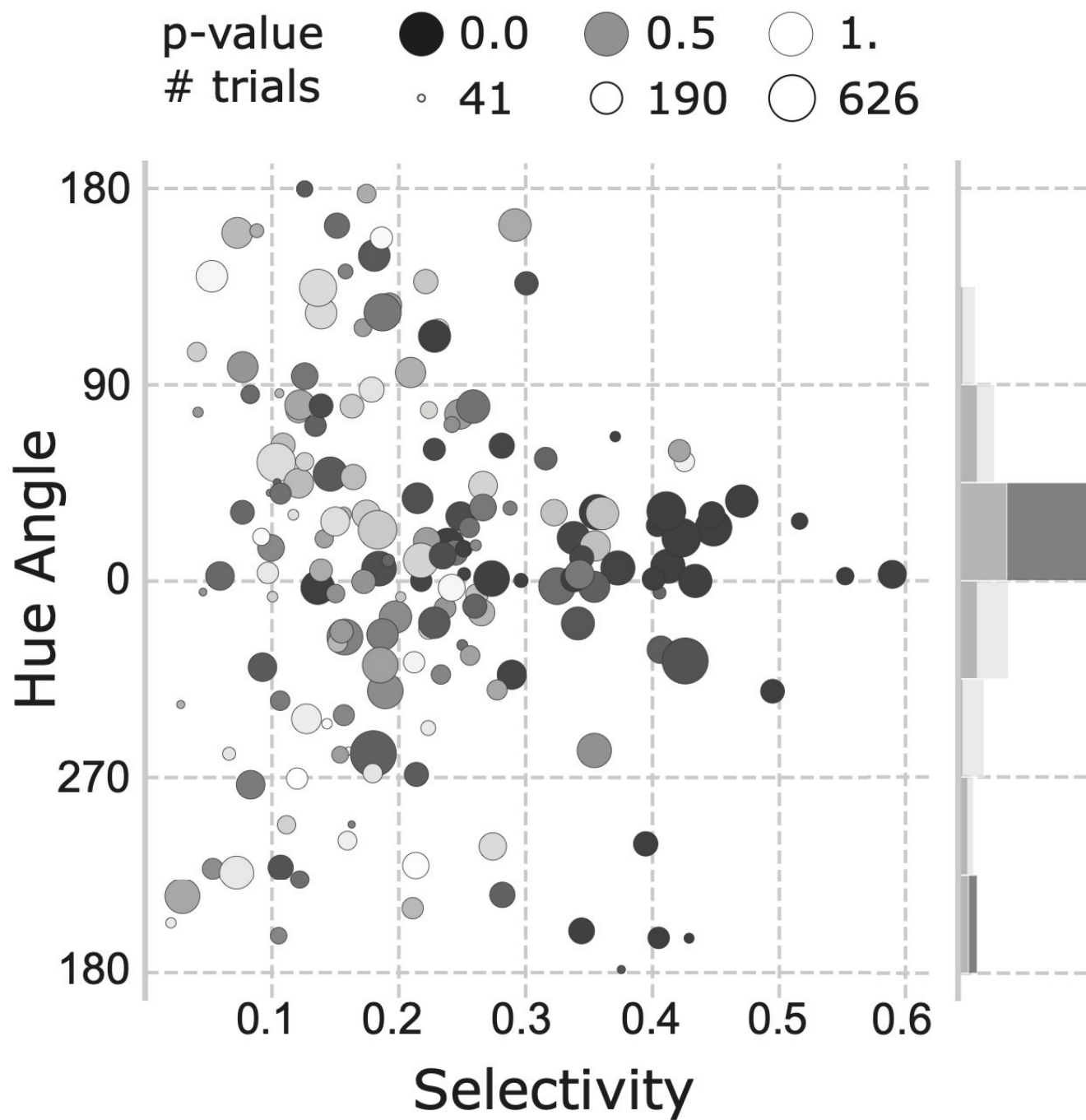
DKL

S

LM

ML

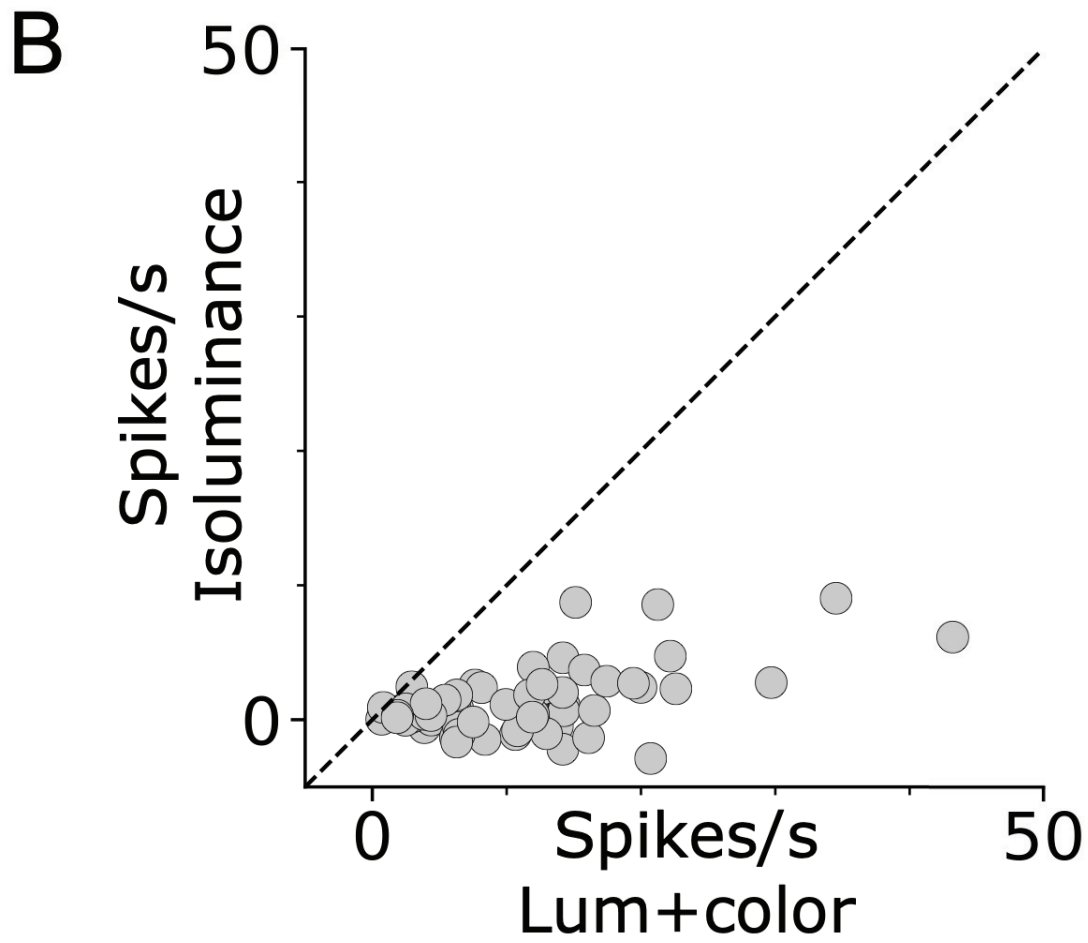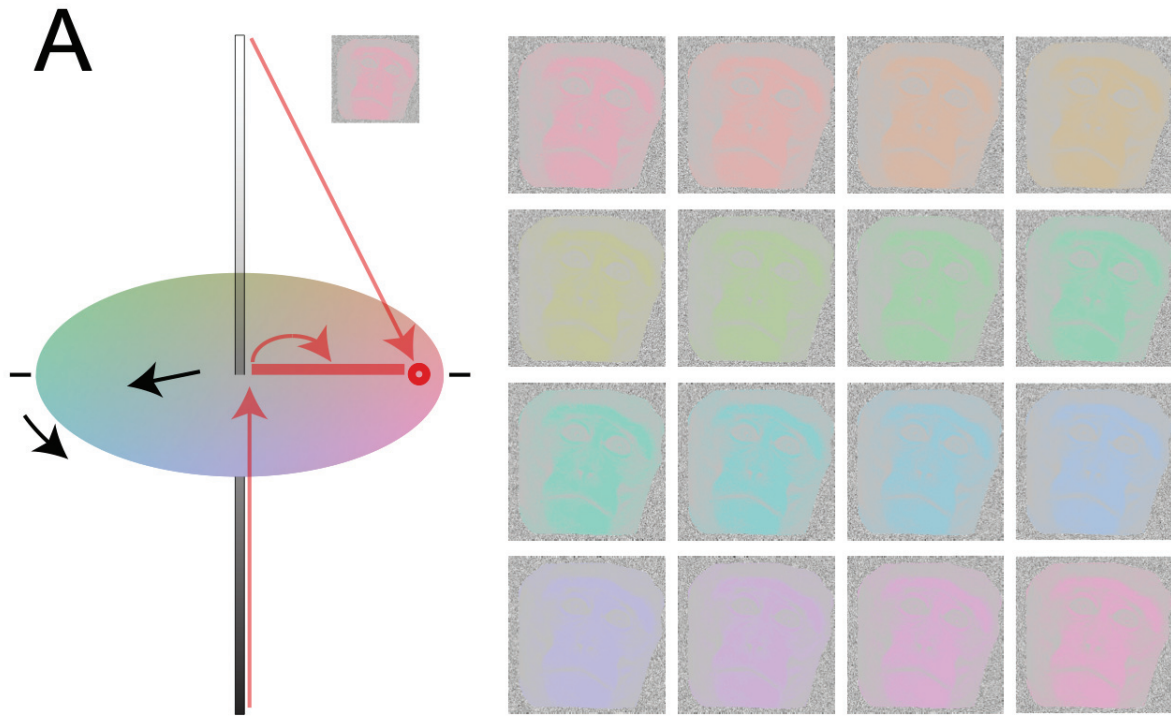AL

Hue angle

Hue angle
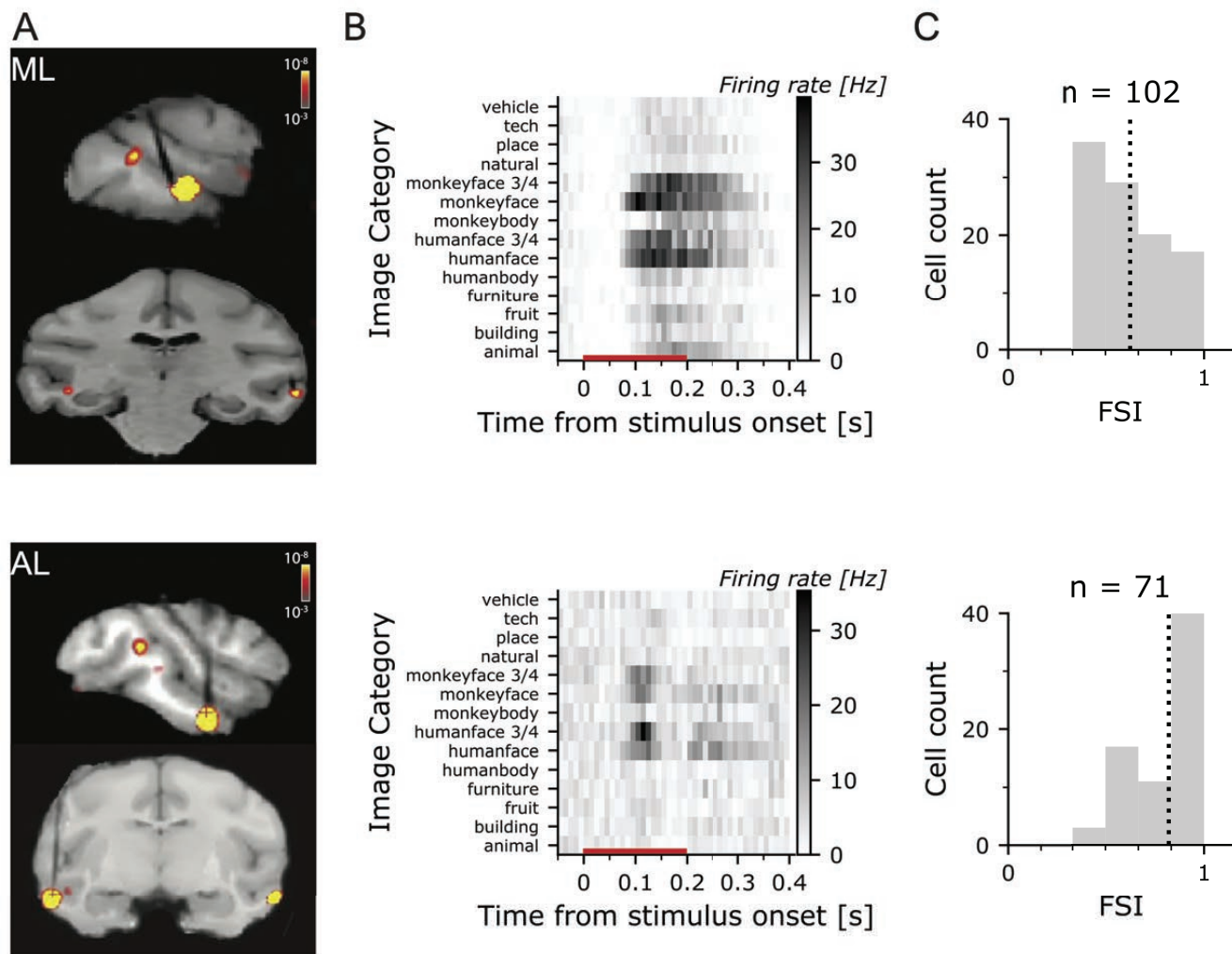
0.2 ■ Cell response
0 □ (normalized firing rate)

0 ■ Color-tuning
>0.1 ■ significance (p value)

A

B

C
M1 M2 M3

first component

#cells

second component

A

B

Firing rate
[spks/sec above baseline]

Time from stimulus
onset [s]

C

fMRI response
[% signal change]

single-cell response
[spks/sec above baseline]

A

Hypothetical cell tuning

Neural response

Hue angle

p

Number of cells

Preferred hue angle
[degrees, L u' v']

w

Full width at half maximum
[degrees, L u' v]

m

Minimum firing rate
[spks/s]

a

Amplitude
[spks/sec]

B

- - - Distribution of face-skin colors

Average neural response [spks/sec]

Hue angle [degrees, L u' v']

0-180 axis

90-270 axis

C

Fisher Information

Hue angle [degrees, L u' v']

0-180 axis

90-270 axis

	M1			*M2*			*M3*			*Total*		
	#cells	latency	duration	#cells	latency	duration	#cells	latency	duration	#cells	latency	duration
ML	45	125	180	57	75	150	-	-	-	102	95	175
AL	7	135	160	15	95	130	49	75	60	71	85	110

	CIE xyY			CIE Luv		DKL	
	x	y	Y	u'	v'	LM	S
white point	0.3009	0.3311	56.5	0.1889	0.4677	0	0
hue 0°	0.3473	0.3183	56.5	0.2268	0.4677	0.0979	0.0547
hue 22.5°	0.3581	0.3427	56.5	0.2239	0.4822	0.0935	0.2145
hue 45°	0.3607	0.3675	56.5	0.2157	0.4945	0.0760	0.3347
hue 67.5°	0.3536	0.3884	56.5	0.2034	0.5027	0.0483	0.4026
hue 90°	0.3370	0.4010	56.5	0.1889	0.5056	0.0145	0.4123
hue 112.5°	0.3137	0.4020	56.5	0.1744	0.5027	-0.0214	0.3637
hue 135°	0.2882	0.3909	56.5	0.1621	0.4945	-0.0550	0.2615
hue 157.5°	0.2659	0.3704	56.5	0.1538	0.4822	-0.0819	0.1164
hue 180°	0.2505	0.3450	56.5	0.1510	0.4677	-0.0979	-0.0547
hue 202.5°	0.2441	0.3196	56.5	0.1538	0.4532	-0.0995	-0.2282
hue 225°	0.2465	0.2980	56.5	0.1621	0.4409	-0.0852	-0.3754
hue 247.5°	0.2563	0.2826	56.5	0.1744	0.4326	-0.0562	-0.4678
hue 270°	0.2717	0.2747	56.5	0.1889	0.4298	-0.0171	-0.4851
hue 292.5°	0.2907	0.2748	56.5	0.2034	0.4326	0.0248	-0.4226
hue 315°	0.3111	0.2826	56.5	0.2157	0.4409	0.0617	-0.2933
hue 337.5°	0.3308	0.2975	56.5	0.2239	0.4532	0.0871	-0.1239